Analyzing the Boundary Equations of Motion for a Holographic Toy Model in AdS_2/CFT_1

Rebecka Mähring
rebecka.mahring@gmail.com

under the direction of
Jorge Laraña Aragón
and Prof. Bo Sundborg
Department of Cosmology, Particle Astrophysics and Strings
Stockholm University

Research Academy for Young Scientists
July 11, 2018

Abstract

The holographic principle and AdS/CFT, are new approaches to unifying quantum mechanics and general relativity. This study investigated the nature of chaos in the boundary of a holographic toy model in AdS_2/CFT_1, and how it depends on different parameters and time intervals. Firstly, the ordinary differential equations describing the toy model were derived using Lagrangian mechanics, and secondly, they were solved numerically to attain the equations of motion for the fields. Perturbations were gradually introduced to the initial values of the differential equations, leading to changes in the trajectories of the fields. These changes were quantified using the Lyapunov exponent, and occasionally identified as chaos. Consequently, it was found that the strength of the coupling between fields contributed to more chaos, instability in one field spreads to the others, and chaos varies depending on the time interval. Additionally, the chaos detected suggests the presence of a massive object, such as a black hole, in the corresponding bulk.

Acknowledgements

First and foremost, I would like to thank my mentor, Jorge Laraña Aragón, for his patience, and willingness to answer my endless questions. Additionally, I want to acknowledge the hard work of this years organizers Jakob Broman, Jonna Karlberg, Jenny Angelin and Hampus Gummesson Svensson, and the contributions of Rays's collaborators AcadeMedia and, Kjell and Märta Beijers Stiftelse, without whom this would have been impossible.

Contents

1 Introduction

Modern physics is divided into two main branches: quantum mechanics, which describes the microscopic parts of reality, and general relativity, which incorporates the macroscopic. Both are true in their respective domains, but ultimately incompatible. The natural step forward is thus a theory incorporating gravity in quantum mechanics, a goal most commonly known as quantum gravity.

Black holes represent one of the few places where both theories are present: quantum mechanics through Hawking radiation [1], and general relativity through the mass and continued implosion of black holes [2]. Because of this intersection between the two wildly different theories, new approaches are needed to tackle problems surrounding black holes.

1.1 Previous Research

In 1974, Stephen Hawking showed that the entropy S_{BH} of a black hole is proportional to the surface area A of its event horizon through the equation

$$S_{BH} = \frac{kA}{4l_p^2}$$

where k is the Boltzman constant, and l_p is the Planck length [3]. This result was surprising, since the entropy of a system is most often dependent on its volume. Furthermore, since the entropy of a black hole is intimately connected to the information it has absorbed, it suggests that the content of a black hole can ultimately be described using only its surface area – which is one dimension lower than the volume.

More recently, the holographic principle – a result of string theory describing connections between systems of higher and lower dimensions – was conjectured by t'Hooft [4] and properly defined by Susskind [5]. Furthermore, Maldacena built on their research by finding the AdS/CFT correspondence [6], which is a special case of the holographic principle. AdS/CFT, especially, has proven a powerful tool for studying strongly interacting fields in quantum field theory, and complex problems involving quantum gravity.

1.2 Aim of Study

The aim of of this study is to investigate the behavior of chaos in the boundary of a holographic toy model in AdS_2/CFT_1. Concretely, this will be done by searching for instability in the classical solutions to the ordinary differential equations of motion describing the oscillating fields contained in the boundary. The insight gained into the workings of the fields in the boundary can then be used to draw conclusions about the gravitational theory contained in the bulk.

1.3 Holography

The holographic principle states that there is a connection between the gravitational theory contained in D spacetime dimensions, and the quantum field theory of D-1 dimensions [5]. The former is referred to as "the bulk", and the latter as "the boundary" [5]. This can be understood by comparison with its namesake: just as a hologram projects a complete three-dimensional picture from a two-dimensional surface using lasers, the lower-dimensional boundary contains encoded information about the higher-dimensional bulk.

The holographic principle has been developed especially through the AdS/CFT correspondence, which is a special case of the principle. It differs mainly from general holography through its stated connection between anti-de Sitter spaces (AdS) – a particular geometric shape of spacetime that differs from our own) in the bulk, and conformal field theories (CFT) – a type of quantum field theory – in the boundary [6].

Since physics is structured around the existence of one time dimension, this is a necessary characteristic of both the bulk and boundary. The simplest system, in terms of number of dimensions, that can be considered is thus a bulk with D=2 (one space dimension and one time dimension), and a corresponding boundary with D=1 (only a time dimension). This special case – when explored through the AdS/CFT correspondence – is described using the notation AdS_2/CFT_1.

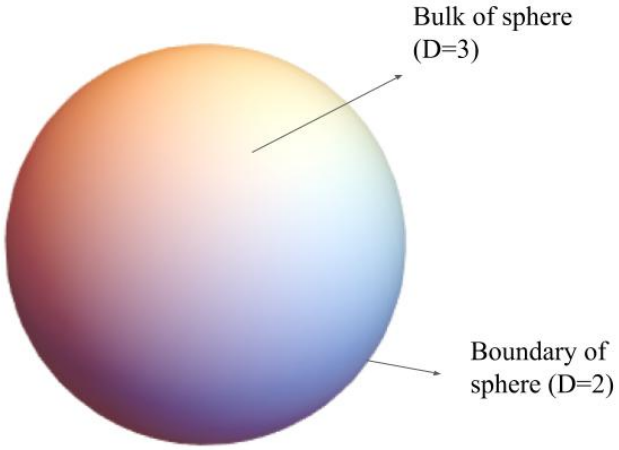

Figure 1: Holography relating to spheres.

1.4 Newtonian and Analytical Mechanics

From Newton's second law of motion $\vec{F} = m\vec{a}$, the motion of an object under uniform acceleration or constant velocity can be derived. Since these equations relate position to its time derivatives velocity and acceleration, they are an example of ordinary differential equations.

However, since Newtonian mechanics is derived from the forces at play, this approach becomes cumbersome when dealing with more complex systems. An alternative way of finding the right equations of motion is through analytical mechanics, and, in particular, through Lagrangian mechanics.

Lagrangian mechanics centeres around a quantity called the Lagrangian L which is, for conservative systems, defined as

$$L = T - V, \tag{1}$$

where V is the potential energy and T is the kinetic energy. The Lagrangian is then implemented to define the Euler-Lagrange partial differential equation, in this case for

one dimension, where φ denotes the sought for function, and $\dot{\varphi}$ its first derivative:

$$\frac{\partial L}{\partial \varphi} - \frac{d}{dt}\left(\frac{\partial L}{\partial \dot{\varphi}}\right) = 0 \tag{2}$$

By manipulating the Lagrangian (equation 1), as defined by the mechanical energy of the system, and the Euler-Lagrange equation (equation 2), the specific equations of motion for the dynamical system can be derived.

1.5 Classical Chaos

Classical chaos is when a dynamical system is sensitive to initial conditions, or, as Edward Lorentz put it, "when the present determines the future, but the approximate present does not approximately determine the future" [7].

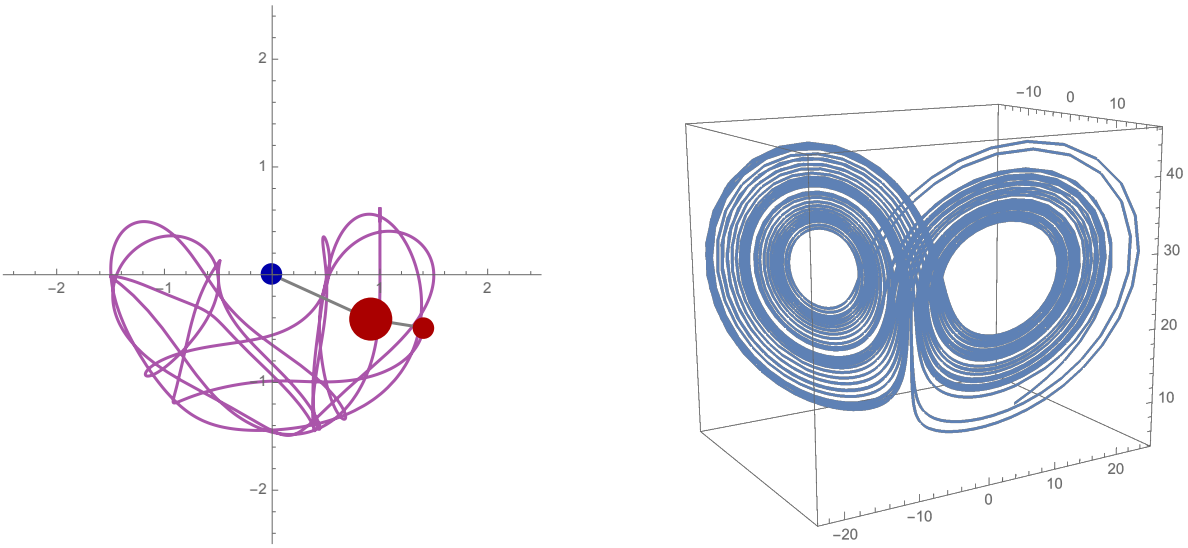

(a) Double pendulum in 2D.

(b) Lorentz attractor in 3D.

Figure 2: Two examples of classical chaos.

While some systems, such as the double pendulum (Figure 2a), have chaotic solutions for all initial values, others are only chaotic in certain intervals. The Lorentz system, which is a simplified model for atmospheric convection, is an example of such as system [7]. As can be seen in Figure 2b, its symmetrical appearance makes it appear ordered, whereas in reality a small change in initial conditions will send a particle in one of two

completely different directions.

Chaos theory can be applied to black holes, and how they interact with their surroundings; e.g., a small change in the initial position or velocity of a particle passing a black hole will result in a different trajectory, and might even lead to it being absorbed by the black hole. Because of this, the equations of motion for a particle or field will display chaotic behavior close to black holes.

1.5.1 Detection and Quantification of Chaos

Chaos can be detected by finding the solution to a differential equation, and then gradually changing the initial conditions and graphing the resulting functions alongside each other. If the graphs differ significantly, then it suggests a high sensitivity to initial conditions – in other words, chaos.

A more rigorous way of detecting and measuring chaos is through the Lyapunov exponent [7]. It characterizes the rate of separation between two solutions to differential equations, or, concretely, between two trajectories. The difference between their initial position is computed and defined as s_0, as is the difference s between their position at the end of the chosen interval. The variable t is then defined as the length of the time interval. These variables are then used to determine the value of λ in the following function:

$$s = s_0 e^{\lambda t}. \tag{3}$$

It is the value of λ that will be analyzed to determine whether the system displays chaotic behavior in the chosen interval: if $\lambda > 0$, then the system is chaotic, whereas if $\lambda \leq 0$, it is stable [7].

A practical way of calculating the Lyapunov exponent is by finding the exponential function $y = ae^{bx}$ that best approximates several coordinates (x, y), where y is the difference between the value of the two graphs at the time x. Since more data points are used in this method, it will often produce a more reliable result.

2 Method

The special case AdS_2/CFT_1 was considered, where the bulk is two-dimensional, and the boundary is one-dimensional. The number of dimensions gave the system two disconnected boundaries, with the bulk in the middle, and the time axes extending infinitely both upwards and downwards.

AdS_3/CFT_2 is the shape of a cylinder, with the boundary wrapped around the bulk, which means that the two parts of the boundary in AdS_2/CFT_1 can reasonably be assumed to be symmetrical. This implies that there should be the same number of fields in both, and that the mass of one field is the same as the one of the corresponding field on the other side. Furthermore, time is assumed to flow in the same direction in the two boundaries, meaning that t can be used as a variable for both.

Since the boundary is divided into two parts, a system of differential equations was needed to describe the fields in the boundary. Specifically, one differential equation was needed for each field in each part of the boundary, meaning that for one field, two second order differential equations were used, and the double amount for two fields.

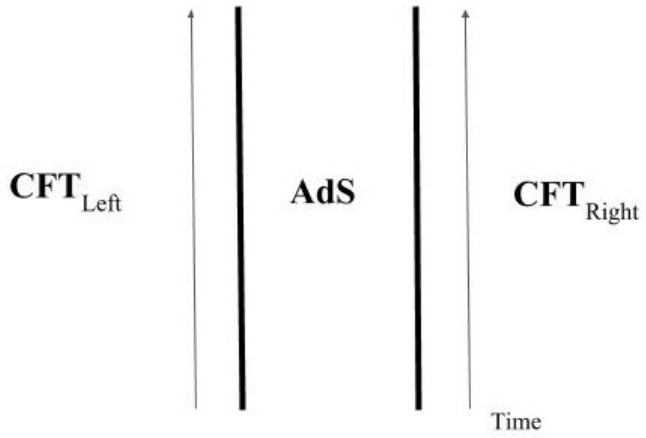

Figure 3: The shape of AdS_2/CFT_1.

The classical limit was imposed on AdS_2/CFT_1, and the dimensions of the boundary were limited to one, meaning that it was possible to work entirely with classical mechanics.

Thus, using the equation for the kinetic energy of a field with mass

$$T = \frac{1}{2}\dot{\varphi}(t)^2 - \frac{1}{2}m^2\varphi(t)^2, \tag{4}$$

the general Lagrangian L could be defined as

$$L = \frac{1}{2}(\dot{\varphi}_L(t)^2 + \dot{\varphi}_R(t)^2 - m_L^2\varphi_L(t)^2 - m_R^2\varphi_R(t)^2) + V_i, \tag{5}$$

where V_i is the potential energy, and the indices L and R denote the the side of the boundary (left or right) the field is oscillating in. Note that the minus sign before V_i was absorbed into the quantity itself. It is now contained in the coupling constant h, which is therefore necessarily a negative number to create a stable system.

The potential energy is dependent on how the fields in the two parts of the boundary are intertwined. Since this study focused on six versions of the holographic toy model where the fields become increasingly intertwined, every system had a unique potential energy, and the Euler-Lagrange equation (see equation 2) produced a specific set of differential equations from which the equations of motion could be derived. Additionally, special attention was paid to how the fields behave – and how chaotic they are – when they are weakly interacting, with the coupling strength h close to zero.

2.1 Lagrangians, and Equations of Motion

Intuitively, the functions and their derivatives describing the fields can be understood as analogous to the equations of motion for a moving particle: the function $\varphi(t)$ describes its trajectory, the first derivative $\dot{\varphi}(t)$ is its velocity, and the second derivative $\ddot{\varphi}(t)$ is its acceleration.

The first version of the system that was considered is referred to as case 0. There is only one field in this version, and the two parts of the boundary are entirely disconnected.

Therefore, the potential $V_0 = 0$, and the Lagrangian was simply

$$L_0 = \frac{1}{2}(\dot{\varphi}_L(t)^2 + \dot{\varphi}_R(t)^2 - m_L^2\varphi_L(t)^2 - m_R^2\varphi_R(t)^2). \tag{6}$$

Hence, the differential equations for the left and right part of the boundary were

$$\text{Case 0}: \quad \begin{cases} \ddot{\varphi}_L(t) + m_L^2\varphi_L(t) = 0 \\ \ddot{\varphi}_R(t) + m_R^2\varphi_R(t) = 0, \end{cases} \tag{7}$$

where m_L and m_R denote the mass terms of fields in the left and right side of the boundary, respectively. Mathematically, they are the parameters of the equations.

In case 1, the number of fields N was still equal to one, but the two parts of the boundary were linked. The potential was therefore no longer equal to zero, but rather defined as the quadratic mixing potential

$$V_1 = h\varphi_L(t)\varphi_R(t), \tag{8}$$

where the coupling constant h was introduced as a new parameter, and could be said to denote the strength of the coupling. Thus, the Lagrangian was

$$L_1 = \frac{1}{2}(\dot{\varphi}_L(t)^2 + \dot{\varphi}_R(t)^2 - m_L^2\varphi_L(t)^2 - m_R^2\varphi_R(t)^2) + h\varphi_L(t)\varphi_R(t). \tag{9}$$

It can be seen in the resulting equations of motion that the two parts of the boundary are now linked, since terms from both the right and left side of the boundary are mixed in the expressions

$$\text{Case 1}: \quad \begin{cases} \ddot{\varphi}_L(t) + m_L^2\varphi_(t) = h\varphi_R(t) \\ \ddot{\varphi}_R(t) + m_R^2\varphi_(t) = h\varphi_L(t). \end{cases} \tag{10}$$

When there is only one field, the next two versions of the toy model – called case 2a and

2b, respectively – had the quadratic potential

$$V_2 = h\varphi_L(t)^2\varphi_R(t)^2, \tag{11}$$

and the shared Lagrangian

$$L_2 = \frac{1}{2}(\dot{\varphi}_L(t)^2 + \dot{\varphi}_R(t)^2 - m_L^2\varphi_L(t)^2 - m_R^2\varphi_R(t)^2) + h\varphi_L(t)^2\varphi_R(t)^2. \tag{12}$$

This gives the resulting set of differential equations:

$$\text{Case 2}: \quad \begin{cases} \ddot{\varphi}_L(t) + m_L^2\varphi_L(t) = 2h\varphi_R(t)^2\varphi_L(t) \\ \ddot{\varphi}_R(t) + m_R^2\varphi_R(t) = 2h\varphi_L(t)^2\varphi_R(t) \end{cases} \tag{13}$$

This version of the holographic model is called case 2. When the number of fields was increased to two, however, case 2a and 2b differed both in terms of potentials and equations of motion. For case 2a, the (now quartic) mixing potential was expressed as

$$V_{2a} = h[\varphi_R(t)]^2[\varphi_L(t)]^2, \tag{14}$$

with the Lagrangian being

$$L_{2a} = \frac{1}{2}(\dot{\varphi}_L(t)^2 + \dot{\varphi}_R(t)^2 - m_L^2\varphi_L(t)^2 - m_R^2\varphi_R(t)^2) + h[\varphi_R(t)]^2[\varphi_L(t)]^2, \tag{15}$$

and the resulting system of differential equations

$$\text{Case 2a}: \quad \begin{cases} \ddot{\varphi}_L(t)_a + m_L^2\varphi_L(t)_a = 2h[\varphi_R(t)_b\varphi_R(t)_b]\varphi_L(t)_a \\ \ddot{\varphi}_R(t)_a + m_R^2\varphi_R(t)_a = 2h[\varphi_L(t)_b\varphi_L(t)_b]\varphi_R(t)_a. \end{cases} \tag{16}$$

In terms of notation, it is important to note that when it is written $[\varphi(t)_b\varphi(t)_b]$, this

stands for the following sum:

$$\sum_{b=1}^{N} \varphi(t)_b \varphi(t)_b = \varphi(t)_1 \varphi(t)_1 + ... + \varphi(t)_N \varphi(t)_N, \tag{17}$$

where the value of b and a denote the vector component, and N is the number of fields.

For case 2b, the potential was

$$V_{2b} = h[\varphi_R(t)\varphi_L(t)]^2, \tag{18}$$

with the Lagrangian being defined as

$$L_{2b} = \frac{1}{2}(\dot{\varphi}_L(t)^2 + \dot{\varphi}_R(t)^2 - m_L^2\varphi_L(t)^2 - m_R^2\varphi_R(t)^2) + h[\varphi_R(t)\varphi_L(t)]^2. \tag{19}$$

Its equations of motion were then derived from the following system of differential equations:

$$\text{Case 2b}: \quad \begin{cases} \ddot{\varphi}_L(t)_a + m_L^2\varphi_L(t)_a = 2h[\varphi_L(t)_b\varphi_R(t)_b]\varphi_R(t)_a \\ \ddot{\varphi}_R(t)_a + m_R^2\varphi_R(t)_a = 2h[\varphi_L(t)_b\varphi_R(t)_b]\varphi_L(t)_a. \end{cases} \tag{20}$$

To describe the activity in the boundary, one equation of motion is needed for each field. Therefore, case 2a and 2b both had four solutions to their differential equations. The two solutions of the left were called $\varphi_L(t)$ and $\varphi_L(t)_2$, and the ones for the right were $\varphi_R(t)$ and $\varphi_R(t)_2$.

The last variation of the dynamical system that was considered is called case 3. Here, the two parts of the boundary were interwoven in even more complex ways, and several new coupling constants – h_2, h_4, $h_{2,2}$ and $\tilde{h}_{2,2}$ – were introduced. Together with the mass terms of the fields, they were tuned to create a stable system. In this study, negative numbers were used for the coupling constants, and, because of the Higgs mechanism, the mass terms were set equal to imaginary numbers.

This connection between the two parts of the boundary can be seen in the new potential:

$$V_3 = h_2\varphi_L(t)\varphi_R(t) + h_4\varphi_L(t)^4 + h_4\varphi_R(t)^4 + h_{2,2}\varphi_L(t)^2\varphi_R(t)^2 + \tilde{h}_{2,2}(\varphi_L(t)\varphi_R(t))^2 \quad (21)$$

and the Lagrangian

$$\begin{aligned} L_3 = \frac{1}{2}(\dot{\varphi}_L(t)^2 + \dot{\varphi}_R(t)^2 - m_L^2\varphi_L(t)^2 - m_R^2\varphi_R(t)^2) + h_2\varphi_L(t)\varphi_R(t) + h_4\varphi_L(t)^4 \\ +h_4\varphi_R(t)^4 + h_{2,2}\varphi_L(t)^2\varphi_R(t)^2 + \tilde{h}_{2,2}(\varphi_L(t)\varphi_R(t))^2 \end{aligned} \quad (22)$$

From which the following system of two equations could be derived:

$$\text{Case 3 :} \quad \begin{cases} \ddot{\varphi}_R(t)_a + m_R^2\varphi_R(t)_a = h_2\varphi_L(t)_a + 4h_4[\varphi_R(t)_b\varphi_R(t)_b]\varphi_R(t)_a + \\ \qquad 2h_{2,2}[\varphi_L(t)_b\varphi_L(t)_b]\varphi_R(t)_a + 2\tilde{h}_{2,2}[\varphi_L(t)_b\varphi_R(t)_b]\varphi_L(t)_a \\ \ddot{\varphi}_L(t)_a + m_L^2\varphi_L(t)_a = h_2\varphi_R(t)_a + 4h_4[\varphi_L(t)_b\varphi_L(t)_b]\varphi_L(t)_a + \\ \qquad 2h_{2,2}[\varphi_R(t)_b\varphi_R(t)_b]\varphi_L(t)_a + 2\tilde{h}_{2,2}[\varphi_R(t)_b\varphi_L(t)_b]\varphi_R(t)_a. \end{cases} \quad (23)$$

2.2 Implementing Wolfram Mathematica

The differential equations belonging to the first two variations (case 0 and case 1) of the dynamical system were solveable analytically, but not those with a higher number of fields and more complicated mixing potentials. Therefore, the command "NDSolveValue" was used in the programming language Wolfram Mathematica to solve the equations numerically. Every second order differential equation needed to be rephrased in terms of two first order differential equations, and every parameter and initial value was defined as a variable that could be easily manipulated in a chosen interval. A simple computer program was then used to determine the largest Lyapunov exponent, and, thereby, to search for chaos.

2.3 General Approach

The same initial value – specifically, $\dot{\varphi}_L(t_0)$ – was varied across all cases. The Lyapunov exponent was then calculated both for the function whose initial value was varied, and for the ones whose initial values were kept constant. This made it possible to see how changes in one function affects the others, and how the subsequent chaos varies across fields. Furthermore, the Lyapunov exponent was calculated for two time intervals: between 0 and 10, and between 90 and 100. Therefore, the results could be compared and used to draw conclusions about whether the fields are more sensitive to initial conditions when they have recently begun oscillating.

The mass terms m_R and m_L were kept at the constant value 1 for all cases except 3, where they were assigned the value i. Because of this, the effect of the mass of the fields on the fields' sensitivity to initial conditions was not studied. However, the constants denoting the strength of the coupling (h, h_2, h_4, $h_{2,2}$ and $\tilde{h}_{2,2}$) were all varied together between -0.1, -0.5, and -1. Thus, it could be studied whether the strength of the coupling between fields affect their stability. This study focused especially on weakly interacting fields, since the program solving the equations numerically proved unreliable for larger values.

3 Results and Discussion

3.1 One field

The first three versions of the toy model (case 0, case 1, and case 2) all contain one field in each part of the boundary. For each case, a total of two functions describing the trajectories of fields were studied.

3.1.1 Case 0

Since the two sides of the boundary are not linked in case 0, the system of differential equations consists of two expressions that are fundamentally the same, and that do not affect each other. Therefore, it is only necessary to consider one graph.

When the mass term $m > 0$ (see Figure 4a), the graph is a normal harmonic function, with the same amplitude in every time interval. The function is identical to that of a harmonic oscillator. It is still relevant, however, since it contains information about how the fields behave – and how stable they are – when they are not coupled.

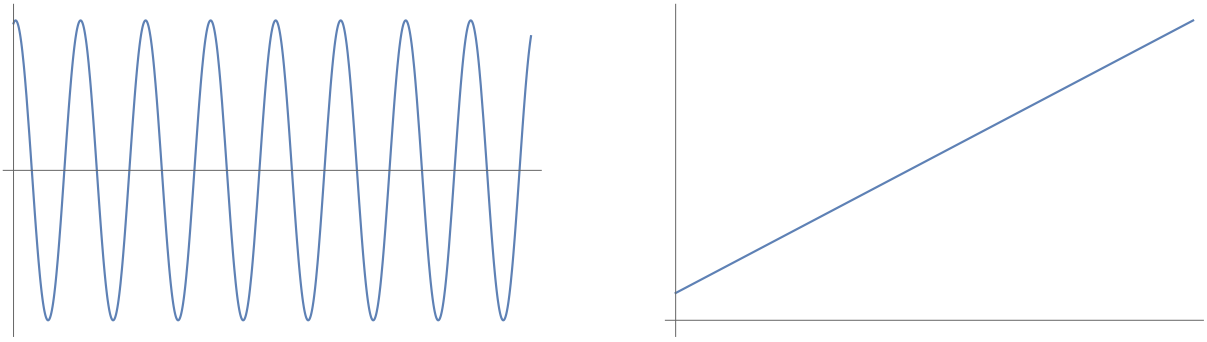

(a) Solution to case 0 for $m > 0$.

(b) Solution to case 0 for $m = 0$.

Figure 4: Two different solutions to case 0.

The graph becomes linear when $m = 0$ (see Figure 4b). This result can be explained mathematically, since Equation 7 is then defined as $\ddot{\varphi}(t) = 0$, which is an ordinary differential equation whose analytical solution is given by

$$\ddot{\varphi}(t) = 0 \Rightarrow \dot{\varphi}(t) = C_1 \Rightarrow \varphi(t) = C_1 t + C_2 \tag{24}$$

where C_1 and C_2 are constants that are determined by the initial values $\varphi(t_0)$ and $\dot{\varphi}(t_0)$ respectively, and the solution $\varphi(t)$ is a linear function.

When the initial conditions of Equation 7 were varied, no dramatic difference was found between the old and new trajectories of the field for any main parameters. The largest Lyapunov exponent of the system was, additionally, consistently below zero. In other words, no chaos was found in the holographic toy model for case 0.

3.1.2 Case 1 and 2

Although case 1 seemed to often display more chaos than case 2 in the chosen intervals, they showed very similar behavior in terms of patterns and trends across different time intervals and values for parameters.

A trend that was especially apparent in case 1 was that chaos seems to grow as the coupling strength h becomes larger (see Figure 5). This result can be related to the absence of chaos in case 0, where the coupling strength is zero.

Another apparent pattern in case 1 and 2 was that the Lyapunov exponent consistently had a larger value for $\varphi_L(t)$ than for $\varphi_R(t)$ – despite the fact that it was the initial velocity $\dot{\varphi}_L(t_0)$ of $\varphi_L(t)$ that was varied, and not that of $\varphi_R(t)$. This correspondence between chaos in the different fields is showcased in Figure 6, where it can be seen that the trajectory of the right field changes alongside the left.

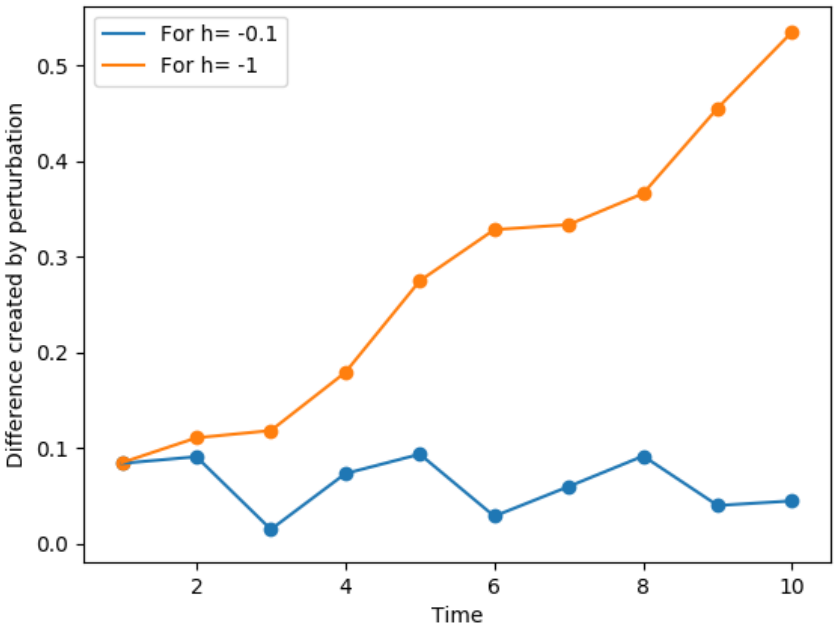

Figure 5: The influence of the coupling strength h on the stability of the field $\varphi_L(t)$ in case 1.

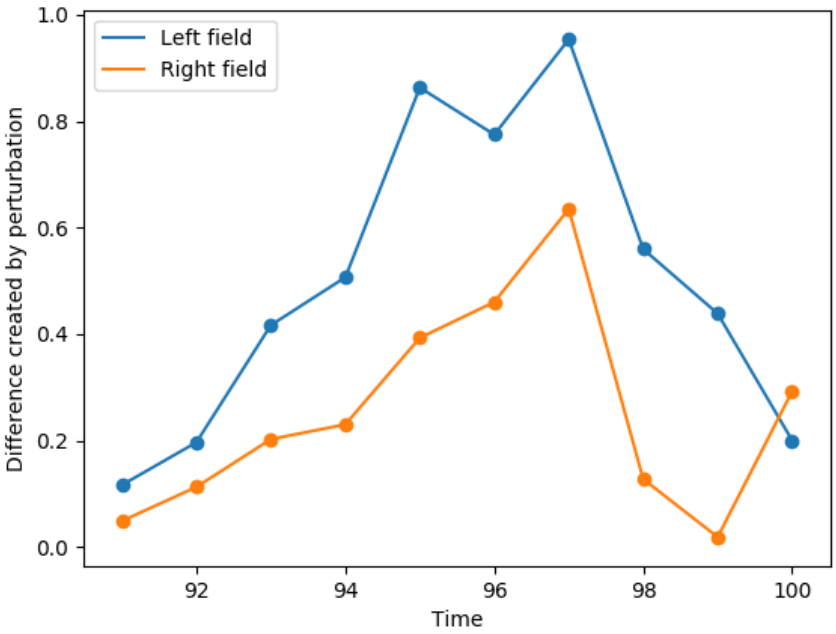

Figure 6: The effect of a perturbation in the initial velocity of the left field on both fields in case 2.

3.2 Two fields

The next three versions of the toy model – case 2a, case 2b, and case 3 – all have two fields in each part of the boundary. The Lypunov was computed for all of the four resulting functions.

3.2.1 Case 2a and 2b

Both case 2a and case 2b were chaotic more consistently than the earlier cases. This is true for case 2b, especially, where every calculated Lyapunov exponent had a positive value. Case 2a also mainly displayed chaos, except for some of the small values for coupling constants.

Case 2a and 2b differ significantly in their results for different time intervals. While the fields in case 2b displayed more chaotic behavior in the earlier time interval than the later one, the fields in case 2a did the opposite, and was usually more stable in the earlier

interval. This result seemed to depend partly on the strength of the coupling as well as which field was being studied.

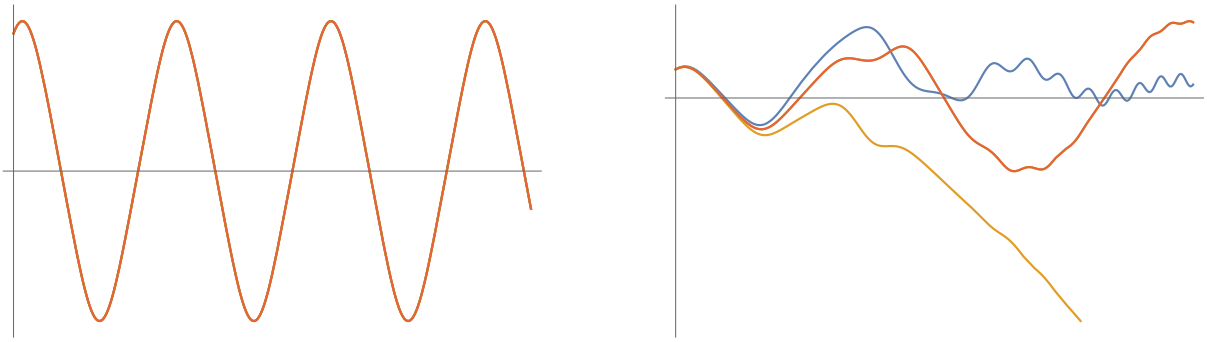

(a) Case 2b, $h = -1$, without perturbation. (b) Case 2b, $h = -1$, with perturbation 0.1.

Figure 7: Chaos in all four fields in case 2b.

Some of the same patterns could be seen in the results as for earlier cases: the fields whose initial values were not changed also displayed chaotic behavior (Figure 7), and an increased value of h seemed to destabilize the system.

3.2.2 Case 3

For case 3, every Lyapunov exponent was positive, meaning that all fields were consistently chaotic for different coupling strengths and time intervals. The Lyapunov exponents were not, however, always larger than chaotic values in other cases. This means that although chaos becomes more common when the fields are more enmeshed, it does not necessarily grow to a larger magnitude.

In case 3, all fields were also affected when the initial value of one was changed, and a larger value of the coupling constant seemed to contribute to more chaos. Additionally, case 3 is similar to case 2b in the sense that it displays more chaos in the earlier time interval than in the later one, implying that the oscillating fields somehow stabilize later.

4 Conclusions and Comparison of Results

The results suggest that the coupling strength h is correlated with the amount of chaos present in the system. In other words, the fields' trajectories are less stable the stronger the coupling between them is. Additionally, as the fields become more strongly coupled, chaos seems to spread more easily from one field to the next.

There also seems to be a connection between how enmeshed and unstable the fields are. This is supported by the fact that in case 3 and case 2b – where the fields are most intertwined – the Lyapunov exponent was always positive. In contrast, systems such as case 1 and case 2, where the fields are more independent of each other, regularly produced negative Lyapunov exponents. This implies that case 3 and 2b are generally more unstable than the earlier ones. The sheer magnitude of chaos in later cases, however, does not seem to necessarily increase, meaning that while a more intertwined system assures chaos, the degree of chaos is more dependent on the strength of those couplings than on the mere existence of them.

Another trend that was present for most fields in several cases, was that the trajectories of the fields were more stable in the later time interval. This was true for $\varphi_L(t)$, especially, as can be seen in Figure 8 for the parameters $h = -1$ and $m = 1$.

The results of this study have implications for the higher-dimensional bulk. Since chaos seems to increase when the two parts of the boundary are linked, these systems are more likely to correspond to an anomaly – such as a black hole – in the gravitational theory of the bulk. Regions of stronger couplings between fields could correspond to similar phenomena.

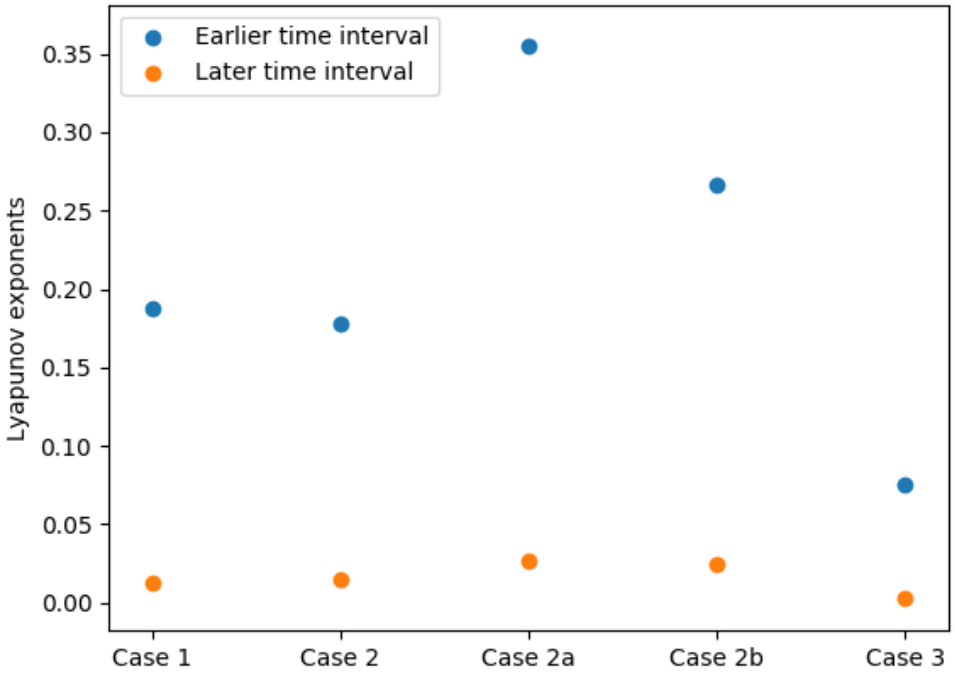

Figure 8: The Lyapunov exponent's dependence on time for $\varphi_L(t)$ in all cases.

4.1 Further Research

The results indicating a correlation between the strength of the coupling and the amount of chaos were not entirely conclusive. This is probably because the value by which h was varied was not large enough to make a significant and consistent difference. To properly evaluate the role of the coupling strength, a larger change in h would be needed between measurements. Additionally, it would be interesting to study the fields when they are more strongly coupled, since chaos should then be more prominent and therefore easier to map. By properly mapping the occurrence and intensity of chaos it would, in turn, become easier to draw conclusions about the gravitational theory in the bulk, since the results in the boundary will then be less ambiguous.

Another aspect of the chosen holographic toy model that would be of interest to study is the impact of the mass terms m_L and m_R on the stability of the oscillating fields, and

how the mass of a field affects the characteristics of the other fields. Furthermore, the different coupling constants in case 3 could be manipulated independently of each other to gain a more nuanced understanding of their impact on the stability of the system.

In the future, the results of this and further studies might be used to draw more detailed conclusions about the gravitational theory contained in the bulk.

References

[1] Hawking, S, *Particle Creation by Black Holes*. Communications in Mathematical Physics, Vol. 43, Iss. 3 (1975).

[2] Wald, R, *Gravitational Collapse and Cosmic Censorship*, Black Holes, Gravitational Radiation and the Universe, p. 69-86 (1997).

[3] Hawking, S, *Black holes and thermodynamics*, Physical Review, Vol. 13, Iss. 2 (1976).

[4] t'Hooft, G, *Dimensional reduction in quantum gravity*, Conf.Proc. C930308 284-296 (1993).

[5] Susskind, L, *The World as a Hologram*, Journal of Mathematical Physics, Vol. 36, Iss. 11 (1994).

[6] Maldancena, J, *The Large N Limit of Superconformal Field Theories and Supergravity*, International Journal of Theoretical Physics, Vol. 38, Iss. 4 (1999).

[7] Strogatz, S, *Nonlinear Dynamics and Chaos: with Applications to Physics, Biology, Chemistry, and Engineering*, Boulder, CO, Westview Press, a member of the Perseus Books Group (2015).

A Computed Lyapunov exponents

For case 0, case 1, case 2, case 2a, and case 2b, the mass terms m_L and m_R were kept constant as $m_L = m_R = 1$. Only case 3 is different, where $m_R = m_L = i$.

For all studied cases, $\dot{\varphi}_L(t)$ was the only initial value that was varied. All other initial values for all functions were set equal to one, and the value of $\dot{\varphi}_L(t)$ was always changed from 1.0 to 1.1. The perturbation was, in other words, always equal to 0.1. Furthermore, the different coupling constants were always set equal to each other, and are in the tables below referred to as h.

A.1 Case 0

Lyapunov exponents for case 0.

Field:	Lyapunov I (0<t<10)	Lyapunov II (90<t<100)
$\varphi_L(t)$	-0.0449104	-0.0010079
$\varphi_R(t)$	-0.0449104	-0.0010079

A.2 Case 1

Lyapunov exponents for case 1.

Field:	Lyapunov I (0<t<10)	Lyapunov II (90<t<100)
$h = -0.1$		
$\varphi_L(t)$	-0.0542488	-0.00131432
$\varphi_R(t)$	0.339719	0.0270412
$h = -0.5$		
$\varphi_L(t)$	-0.121938	-0.00330082
$\varphi_R(t)$	0.238728	0.0208512
$h = -1$		
$\varphi_L(t)$	0.187955	0.0128017
$\varphi_R(t)$	0.370025	0.030741

A.3 Case 2

Lyapunov exponents for case 2.

Field:	Lyapunov I (0<t<10)	Lyapunov II (90<t<100)
$h = -0.1$		
$\varphi_L(t)$	-0.17344	-0.00453689
$\varphi_R(t)$	0.181253	0.0150173
$h = -0.5$		
$\varphi_L(t)$	-0.012793	0.0003564
$\varphi_R(t)$	0.0899473	0.00655707
$h = -1$		
$\varphi_L(t)$	0.177835	0.0153721
$\varphi_R(t)$	0.198185	0.0172361

A.4 Case 2a

Lyapunov exponents for case 2a.

Field:	Lyapunov I (0<t<10)	Lyapunov II (90<t<100)
$h = -0.1$		
$\varphi_L(t)$	-0.214458	-0.00526176
$\varphi_R(t)$	-1.11229	0.00864374
$\varphi_L(t)_2$	-1.08747	0.0445688
$\varphi_R(t)_2$	0.0888808	0.00864374
$h = -0.5$		
$\varphi_L(t)$	0.191252	0.0138955
$\varphi_R(t)$	0.303647	0.0240346
$\varphi_L(t)_2$	0.45171	0.0416442
$\varphi_R(t)_2$	0.303647	0.0240346
$h = -1$		
$\varphi_L(t)$	0.355134	0.0263168
$\varphi_R(t)$	0.271372	0.0264731
$\varphi_L(t)_2$	0.577265	0.0488122
$\varphi_R(t)_2$	0.271372	0.0264731

A.5 Case 2b

Lyapunov exponents for case 2b.

Field:	Lyapunov I (0<t<10)	Lyapunov II (90<t<100)
$h = -0.1$		
$\varphi_L(t)$	0.298063	0.0205919
$\varphi_R(t)$	0.569283	0.047408
$\varphi_L(t)_2$	0.562409	0.045738
$\varphi_R(t)_2$	0.562409	0.045738
$h = -0.5$		
$\varphi_L(t)$	0.22717	0.0199885
$\varphi_R(t)$	0.500342	0.0427717
$\varphi_L(t)_2$	0.572885	0.0516218
$\varphi_R(t)_2$	0.572885	0.0516218
$h = -1$		
$\varphi_L(t)$	0.265941	0.0240991
$\varphi_R(t)$	0.533435	0.0451348
$\varphi_L(t)_2$	0.551337	0.049524
$\varphi_R(t)_2$	0.551337	0.049524

A.6 Case 3

Lyapunov exponents for case 3.

Field:	Lyapunov I (0<t<10)	Lyapunov II (90<t<100)
$h = -0.1$		
$\varphi_L(t)$	0.170231	0.0156184
$\varphi_R(t)$	0.35984	0.0314436
$\varphi_L(t)_2$	0.371827	0.0322954
$\varphi_R(t)_2$	0.403676	0.0375435
$h = -0.5$		
$\varphi_L(t)$	0.00208957	0.000662304
$\varphi_R(t)$	0.0931295	0.00542016
$\varphi_L(t)_2$	0.172255	0.0109546
$\varphi_R(t)_2$	0.247242	0.0186253
$h = -1$		
$\varphi_L(t)$	0.0747887	0.00300936
$\varphi_R(t)$	0.0856808	0.00315493
$\varphi_L(t)_2$	0.173938	0.011355
$\varphi_R(t)_2$	0.543372	0.0473406

B Numerical solutions

B.1 Case 0

```
Manipulate[
 Block[
  {m = p$m, sol$x}, {sol$x} = NDSolveValue[
    {
     D[x[t], t] == v[t],
```

```
      D[v[t], t] == -(m^2*x[t]),
      x[t0] == x0,
      v[t0] == v0},
     {x},
     {t, t0, t1}];
  Row@{
     Plot[{sol$x[t]},
      {t, t0, t1},
      ImageSize -> 400], "   ",
     Style[Table[
          {t, m, sol$x[t]},
          {t, t0, t1, (t1 - t0)/20}]
         // TableForm // N, Blue, 10]}],
 {{t0, 0}, 0, 10},
 {{t1, 10}, 0, 1000},
 {{x0, 1}, 0, 100},
 {{v0, 1}, 0, 100},
 {{p$m, 1}, 0, 10}, SaveDefinitions -> True]
```

B.2 Case 1

```
Manipulate[
 Block[
  {m = p$m, h = p$h, sol$x, sol$z},
  {sol$x, sol$z} = NDSolveValue[
    {
     D[x[t], t] == v[t],
     D[v[t], t] == h*z[t] - m^2*x[t],
     x[t0] == x0,
```

```
    v[t0] == v0,
    D[z[t], t] == u[t],
    D[u[t], t] == h*x[t] - m^2*z[t],
    z[t0] == z0,
    u[t0] == u0
    },
   {x, z},
   {t, t0, t1}
   ];
 Row@{
   Plot[
    {sol$x[t], sol$z[t]},
    {t, t0, t1}, ImageSize -> 400
    ],
   "   ",
   Style[Table[
        {t, m, h, sol$x[t], sol$z[t]},
        {t, t0, t1, (t1 - t0)/20}
        ] // TableForm // N, Blue, 10]
   }
 ],
{{t0, 0}, 0, 10},
{{t1, 10}, 0, 100},
{{x0, 2}, 0, 100},
{{v0, 2}, 0, 100},
{{z0, 2}, 0, 100},
{{u0, 2}, 0, 100},
{{p$m, 1}, 0, 10},
```

```
 {{p$h, 1}, -10, 10}, SaveDefinitions -> True]
```

B.3 Case 2

```
Manipulate[
 Block[
  {m = p$m, h = p$h, sol$x, sol$z},
  {sol$x, sol$z} = NDSolveValue[
    {
     D[x[t], t] == v[t],
     D[v[t], t] == x[t]*(2 h*z[t]^2 - m^2),
     x[t0] == x0,
     v[t0] == v0,
     D[z[t], t] == u[t],
     D[u[t], t] == z[t]*(2 h*x[t]^2 - m^2),
     z[t0] == z0,
     u[t0] == u0
     },
    {x, z},
    {t, t0, t1}
    ];
  Row@{
    Plot[
     {sol$x[t], sol$z[t]},
     {t, t0, t1}, ImageSize -> 400
     ],
    "  ", Style[Table[
        {t, m, h, sol$x[t], sol$z[t]},
        {t, t0, t1, (t1 - t0)/20}
```

```
        ] // TableForm // N, Blue, 10]
    }
  ],
 {{t0, 0}, 0, 10},
 {{t1, 10}, 0, 100},
 {{x0, 1}, 0, 100},
 {{v0, 1}, 0, 100},
 {{z0, 1}, 0, 100},
 {{u0, 1}, 0, 100},
 {{p$m, 1}, 0, 10},
 {{p$h, -5}, -10, 0}, SaveDefinitions -> True]
```

B.4 Case 2a

```
Manipulate[
 Block[
  {m = p$m, h = p$h, sol$x, sol$z, sol$a, sol$c},
  {sol$x, sol$z, sol$a, sol$c} = NDSolveValue[
    {
     D[x[t], t] == v[t],
     D[v[t], t] == 2 h*x[t] (z[t]^2 + c[t]^2) - m^2 x[t],
     D[z[t], t] == u[t],
     D[u[t], t] == 2 h*z[t] (x[t]^2 + a[t]^2) - m^2 z[t],
     x[t0] == x0,
     v[t0] == v0,
     z[t0] == z0,
     u[t0] == u0,
     D[a[t], t] == b[t],
     D[b[t], t] == 2 h*a[t] (z[t]^2 + c[t]^2) - m^2 a[t],
```

```
    D[c[t], t] == d[t],
    D[d[t], t] == 2 h*c[t] (x[t]^2 + a[t]^2) - m^2 c[t],
    a[t0] == a0,
    b[t0] == b0,
    c[t0] == c0,
    d[t0] == d0
    },
   {x, z, a, c},
   {t, t0, t1}
   ];
 Row@{
   Plot[
    {sol$x[t]},
    {t, t0, t1}, ImageSize -> 400
    ],
   "  ",
   Style[Table[
       {t, m, h, sol$x[t], sol$z[t], sol$a[t], sol$c[t]},
       {t, t0, t1, (t1 - t0)/20}
       ] // TableForm // N, Blue, 10]
   }
 ],
{{t0, 0}, 0, 10},
{{t1, 10}, 0, 100},
{{x0, 1}, 0, 100},
{{v0, 1}, 0, 100},
{{z0, 1}, 0, 100},
{{u0, 1}, 0, 100},
```

```
 {{a0, 1}, 0, 100},
 {{b0, 1}, 0, 100},
 {{c0, 1}, 0, 100},
 {{d0, 1}, 0, 100},
 {{p$m, 1}, 0, 10},
 {{p$h, -1}, -10, 0}, SaveDefinitions -> True]
```

B.5 Case 2b

```
Manipulate[
 Block[
  {m = p$m, h = p$h, sol$x, sol$z, sol$a, sol$c},
  {sol$x, sol$z, sol$a, sol$c} = NDSolveValue[
    {
     D[x[t], t] == v[t],
     D[v[t], t] == 2 h*z[t] (z[t] x[t] + a[t] c[t]) - m^2 x[t],
     D[z[t], t] == u[t],
     D[u[t], t] == 2 h*x[t] (z[t] x[t] + a[t] c[t]) - m^2 x[t],
     x[t0] == x0,
     v[t0] == v0,
     z[t0] == z0,
     u[t0] == u0,
     D[a[t], t] == b[t],
     D[b[t], t] == 2 h*c[t] (x[t] z[t] + a[t] c[t]) - m^2 a[t],
     D[c[t], t] == d[t],
     D[d[t], t] == 2 h*a[t] (x[t] z[t] + a[t] c[t]) - m^2 c[t],
     a[t0] == a0,
     b[t0] == b0,
     c[t0] == c0,
```

```
    d[t0] == d0
    },
   {x, z, a, c},
   {t, t0, t1}
   ];
 Row@{
   Plot[
    {sol$x[t], sol$z[t], sol$a[t], sol$c[t]},
    {t, t0, t1}, ImageSize -> 400
    ],
   "  ",
   Style[Table[
       {t, m, h, sol$x[t], sol$z[t], sol$a[t], sol$c[t]},
       {t, t0, t1, (t1 - t0)/20}
       ] // TableForm // N, Blue, 10]
   }
 ],
{{t0, 0}, 0, 10},
{{t1, 10}, 0, 100},
{{x0, 1}, 0, 100},
{{v0, 1}, 0, 100},
{{z0, 1}, 0, 100},
{{u0, 1}, 0, 100},
{{a0, 1}, 0, 100},
{{b0, 1}, 0, 100},
{{c0, 1}, 0, 100},
{{d0, 1}, 0, 100},
{{p$m, 1}, 0, 10},
```

```
 {{p$h, -5}, -10, 0}, SaveDefinitions -> True]
```

B.6 Case 3

```
Manipulate[
 Block[
  {m = p$m, h1 = p$h1, h2 = p$h2, h3 = p$h3, h4 = p$h4, sol$x, sol$z,
   sol$a, sol$c},
  {sol$x, sol$z, sol$a, sol$c} = NDSolveValue[
    {
     D[x[t], t] == v[t],
     D[v[t], t] ==
      h1*z[t] + 4 h2*x[t] (x[t]^2 + a[t]^2) +
       2 h3*x[t] (z[t]^2 + c[t]^2) +
       2 h4*z[t] (z[t] x[t] + c[t] a[t]) - m^2 x[t],
     D[z[t], t] == u[t],
     D[u[t], t] ==
      h1*x[t] + 4 h2*z[t] (z[t]^2 + c[t]^2) +
       2 h3*z[t] (x[t]^2 + a[t]^2) +
       2 h4*x[t] (x[t] z[t] + a[t] c[t]) - m^2 z[t],
     x[t0] == x0,
     v[t0] == v0,
     z[t0] == z0,
     u[t0] == u0,
     D[a[t], t] == b[t],
     D[b[t], t] ==
      h1*c[t] + 4 h2*a[t] (x[t]^2 + a[t]^2) +
       2 h3*a[t] (z[t]^2 + c[t]^2) +
       2 h4*c[t] (z[t] x[t] + c[t] a[t]) - m^2 a[t],
```

```
    D[c[t], t] == d[t],
    D[d[t], t] ==
     h1*a[t] + 4 h2*c[t] (z[t]^2 + c[t]^2) +
      2 h3*c[t] (x[t]^2 + a[t]^2) +
      2 h4*a[t] (x[t] z[t] + a[t] c[t]) - m^2 c[t],
    a[t0] == a0,
    b[t0] == b0,
    c[t0] == c0,
    d[t0] == d0
    },
   {x, z, a, c},
   {t, t0, t1}
   ];
 Row@{
   Plot[
    {sol$x[t]},
    {t, t0, t1}, ImageSize -> 400
    ],
   "  ",
   Style[Table[
       {t, m, h1, h2, h3, h4, sol$x[t], sol$z[t], sol$a[t], sol$c[t]},
       {t, t0, t1, (t1 - t0)/20}
       ] // TableForm // N, Blue, 10]
   }
 ],
{{t0, 0}, 0, 100},
{{t1, 10}, 0, 100},
{{x0, 1}, 0, 100},
```

```
{{v0, 1}, 0, 100},
{{z0, 1}, 0, 100},
{{u0, 1}, 0, 100},
{{a0, 1}, 0, 100},
{{b0, 1}, 0, 100},
{{c0, 1}, 0, 100},
{{d0, 1}, 0, 100},
{{p$m, 5 I}, 0, 10 I},
{{p$h1, -5}, -10, 0},
{{p$h2, -5}, -10, 0},
{{p$h3, -5}, -10, 0},
{{p$h4, -5}, -10, 0}, SaveDefinitions -> True]
```